Supplementary Materials for

An Actin-Dependent Step in Mitochondrial Fission Mediated by the ER-Associated Formin INF2

Farida Korobova, Vinay Ramabhadran, Henry N. Higgs*

*To whom correspondence should be addressed. E-mail: henry.higgs@dartmouth.edu

Published 25January 2013, *Science* **339**, 464 (2013)
DOI: 10.1126/science.1228360

This PDF file includes

Other Supplementary Material for this manuscript includes the following:
(available at www.sciencemag.org/cgi/content/full/339/6118/464/DC1)

Movies S1 to S6

Materials and Methods

Plasmids and siRNA oligonucleotides

The human full length GFP-INF2 CAAX constructs was described previously (*13*). All point mutations were made using the QuikChange mutagenesis kit (Stratagene, Santa Clara, CA). The ER-green construct, containing the ER-targeting sequence (amino acids 233–250) of budding yeast UBC6 (*20*), was a gift from Victoria Allan (University of Manchester, Manchester, United Kingdom). CFP-Sec61β was a gift from Jennifer Lippincott-Schwartz (National Institute Health, Bethesda, MD). Mito-dsRed was a gift from Ekta Chhabra (Massachusetts General Hospital). CFP-Drp1 K38E was a gift from Michael Zick.

Oligonucleotides for human total INF2 siRNA were synthesized by IDT Oligo against target sequence 5'- GGAUCAACCUGGAGAUCAUCCGC-3' (siRNA#1), and 5'-GCAGUACCGCUUCAGCAUUGUCA-3' (siRNA#2). Oligonucleotides for INF2 CAAX isoform were 5'-ACAAAGAAACTGTGTGTGA-3' (siRNA#1), and 5'-CCCTGATTCTGATGATAAT-3' (siRNA#2). Oligonucleotides for human Drp1siRNA were synthesized by IDT Oligo against target sequence 5'-GCCAGCUAGAUAUUAACAACAAGAA-3' (siRNA#1) and 5'-GGAACGCAGAGCAGCGGAAAGAGCT-3' (siRNA#2). As a control, Silencer Negative Control #1 siRNA (Ambion) was used.

Cell culture, transfections and drug treatment

NIH 3T3 cells and U2OS cell lines were grown in DMEM (Invitrogen) supplemented with 10% calf serum (Atlanta Biologicals). Cells were seeded at $2x10^5$ cells per well of a 6-well dish ~16 hours prior to transfection. Plasmid transfections were performed in OPTI-MEM media (Invitrogen) with 2 μL Lipofectamine 2000 (Invitrogen) per well. For all experiments, the following amounts of DNA were transfected per well: 30 ng mito-dsRed; 60 ng CFP-Sec61β; 100 ng for all INF2 constructs; 100 ng Drp1 K38E. In the case of simultaneous INF2 and Drp1 transfection, 100 ng for each plasmid was used. For RNAi transfections, cells were plated on 6 well plates with 30-40% density, and 2 μl RNAmax (Invitorgen) and 63 pg of siRNA were used per one well. Cells were analyzed 24 hr and 72-80 hr postransfection for DNA and RNAi respectively. When needed, cells were treated with MitoTracker Red CMXRos (Invitrogen) at 100 nM in DMEM for 20 min prior to fixation. Preparation of U2OS cells stably expressing GFP-INF2-CAAX was described in (*13*). For Latrunculin B (LatB) treatment, cells were plated on poly-L-lysine-coated coverslips (0.1 mg/ml >300,000 MW, Sigma/Aldrich), and transfected with INF2-A149D or INF2-A149D/I643A plasmid the day before treatment. Cells were incubated with medium containing 0.5 μM LatB (from a 2 mM stock in DMSO, medium was pre-equilibrated for temp and CO_2 content before use) for 30 or 60 min, with DMSO used as the negative control.

Antibodies

Polyclonal antibodies against human INF2 N-terminus (amino acids 1-424) or FH1-FH2-C (amino acids 469-1249, CAAX) were raised in rabbits by Covance (Denver, PA), and affinity purified using DID construct (amino acids 1-269) or FH1-FH2 (amino acids 469-940) coupled to Sulfolink (Thermo/Pierce). Production of splice variant-specific

antibodies against human INF2 CAAX (acetyl-EEVPPDSDDNKTKKLC-amide) or nonCAAX (acetyl-CQEGLRPRPKAK) peptides was described in (*13*). Anti-Tubulin (DM1-α, Sigma) was used at 1:10,000 dilution. Drp1 was detected using a rabbit monoclonal antibody (Cell Signaling) at 1:50 dilution. GM130 (Abcam) was detected using a rabbit polyclonal antibody at 1:250 dilution. Secondary antibodies used were Cy5 or Fluorescein conjugated anti-rabbit IgG, (Jackson Immunoresearch and Vector Laboratories, respectively), and used at 1:300 dilution.

Immunofluorescence Microscopy

Cells were fixed with 4% formaldehyde (Electron Microscopy Sciences, PA) in phosphate-buffered saline (PBS) for 30 min at room temperature. After washing with PBS, cells were permeabilized with 0.1% Triton X-100 in PBS for 15 min. Cells were then washed with PBS, blocked with 0.5% BSA in PBS for 1 hr, and incubated with primary antibodies in PBS for 1 hr at room temperature. After washing with PBS, secondary antibodies were applied for 1hr at room temperature. When needed, 500 nM AlexaFluor660-phalloidin (Invitrogen) or 100 nM TRITC-phalloidin (Sigma/Aldrich), and 10 μM 4,6-diamidino-2-phenylindole (DAPI) were added to secondary antibody solution. Samples were mount on polyvinyl alcohol-DABCO.

Live imaging and confocal microscopy

Imaging of live and fixed cells was performed using spinning disk or laser scanning confocal systems. For live imaging, cells grown on 18 mm coverslips were mounted into Rose chambers, then onto a Wave FX spinning disk confocal microscope (Quorum Technologies, Inc., Guelph, Canada, on a Nikon Eclipse Ti microscope) with Bionomic Controller (20/20 Technology, Inc) temperature-controlled stage set to 37°C. After equilibrating to temperature for 10 min, cells were imaged with the 60x 1.4 NA Plan Apo objective (Nikon) using the 403 nm and 450/50 filter for DAPI, 491 nm laser and 525/20 filter for GFP, and the 561 nm laser and 593/40 filter for mRFP. To visualize dynamic structures in volume and time, 5-11 z-stacks of 0.2 μm were collected for each color and each time point, at 5 sec intervals for 4-7 minutes. Maximum intensity projections from best focus Z slices were assembled using Metamorph software and processed using Nikon Elements and Photoshop CS (Adobe, San Jose, CA).

For fixed samples, the laser scanning Nikon A1RSi Confocal Workstation with PMT DU4 and Galvano scanner, and lasers 405, 488, 561 and 639.5 nm was used, attached to Nikon Eclipse Ti inverted microscope. Images were taken as 1024x1024 pixels with PlanApoVC 60x oil objective (NA 1.4), and a pinhole of 1 airy unit. 3D reconstructions were generated in Nikon NIS-Elements AR (3.22.11) from 9 consecutive z-steps of 0.12 μm using the alpha blending option.

Immunoprecipitation and Western blotting

For immunoprecipitations (IP), U2OS cells (100 mm plate at 90% confluence) were lysed at +4°C in 2.5 mL of cold PBS containing Roche Complete Protease inhibitors, 10 mM DTT and 4% SDS. Lysates were immediately boiled 5 minutes, cooled for 1 minute in 23°C water, then 1/10th volume of 300 mM N-ethylmaleimide (NEM, Thermo/Pierce. Freshly made in water) was added. "Thesit" (nonaethylene glycol monododecyl ether, Sigma P-9641) was added to 9% from a 20% stock in water, then the sample was

centrifuged at 100,000 rpm for 20 minutes in a TLA120 rotor (Beckman). The resulting homogenates were pre-cleared using Protein A sepharose beads (GE Biosciences) for 2 hours at 4°C. The IPs were carried out overnight at 4°C using 2 μg of the appropriate antibody and 25 μL of Protein A sepharose beads per mL homogenate. The beads were washed multiple times with PBS (lacking the SDS and DTT but containing 1% thesit) before being processed for SDS-PAGE and western blotting.

To prepare samples for SDS-PAGE, cells were grown on 6 well plate, trypsinized, washed with PBS and resuspended 50 μL PBS. 50 μL was mixed with 34 μL of 10% SDS and 1 μL of 1 M DTT, boiled 5 minutes, cooled to 23°C, then 17 μl of 300 mM of freshly made NEM in water was added. Just before SDS-PAGE, the protein sample was mixed 1:1 with 2xDB (250 mM Tris-HCl pH 6.8, 2 mM EDTA, 20% glycerol, 0.8% SDS, 0.02% bromophenol blue, 1000 mM NaCl, 4 M urea). Proteins were separated by 7.5% SDS-PAGE and transferred to a PVDF membrane (polyvinylidine difluoride membrane, Millipore). The membrane was blocked with TBS-T (20 mM Tris-HCl, pH 7.6, 136 mM NaCl, and 0.1% Tween-20) containing 3% BSA (Research Organics) for 1 hour, then incubated with the primary antibody solution at 4°C overnight. After washing with TBS-T, the membrane was incubated with horseradish peroxidase (HRP)-conjugated secondary antibody (Bio-Rad) for 1 hour at room temperature. Signals were detected by Chemiluminescence (Pierce).

Mitochondria length and Drp1 puncta analysis

To measure mitochondrial length, maximum intensity projections of z-series with 0.2 μm increments for red channel (Mitotracker or mito-dsRed) were created. The flat regions of cells with clearly resolved mitochondria were selected, and 25-30 mitochondria per cell were measured using the line tool in Nikon Elements software. Drp1 puncta were counted on fixed cells labeled with anti-Drp1 antibody. Only mitochondria-associated puncta were quantified, and their association with mitochondria was verified on consecutive z-planes. Statistic analysis was performed in Excel (Microsoft), data presented as mean ± standard error or standard deviation from at least two experiments. Unpaired Student's t-test was used to compare values with $p<0.01$ considered significant.

Actin analysis at ER/mitochondrial contact sites

U2OS cells transfected with WT INF2 or INF2-A149D (GFP-fusion, CAAX variants) were labeled with MitoTracker, fixed and stained with Alexa660-phalloidin, as described above. Cells were imaged by laser scanning confocal microscopy, acquiring Z-stacks of 100 nm steps. Due to abundant cytoplasmic actin filaments, images were first analyzed to locate regions containing mitochondria but with low amounts of stress fibers or other clear non-associated phalloidin staining. These regions were then reconstructed in 3-D using alpha blending algorithm and analyzed sequentially for: evidence of ER-mitochondrion association, with either partial of full circumscription around the mitochondrion; and evidence for actin enrichment at these ER/mitochondrial contact sites. Events were scored as positive for actin accumulation if phalloidin staining occurred at the ER/mitochondrial contact site in several consecutive planes from the reconstruction. A number of events were scored as "unclear" because of evidence that the phalloidin enrichment could be coming from adjacent actin-containing structures.

Microtubule pelleting assays

Conducted following methods described in detail in (19). INF2-FH1FH2C constructs (amino acids 469-1249 of human CAAX variant) for WT and I643A mutant were expressed in bacteria and purified. Pelleting assays using taxol-stabilized porcine brain microtubules (0.5 μM) were conducted at 23˚C in 10 mM imidazole pH 7, 50 mM KCl, 1 mM EGTA, 1 mM MgCl2, 1 mM DTT, 0.1 mM GTP, 20 μM paclitaxel (Calbiochem, La Jolla CA) and 0.5 mM thesit. Centrifugation at 23˚C and 60,000 rpm for 15 min in a TLA-100 rotor (Beckman-Coulter, Brea CA).

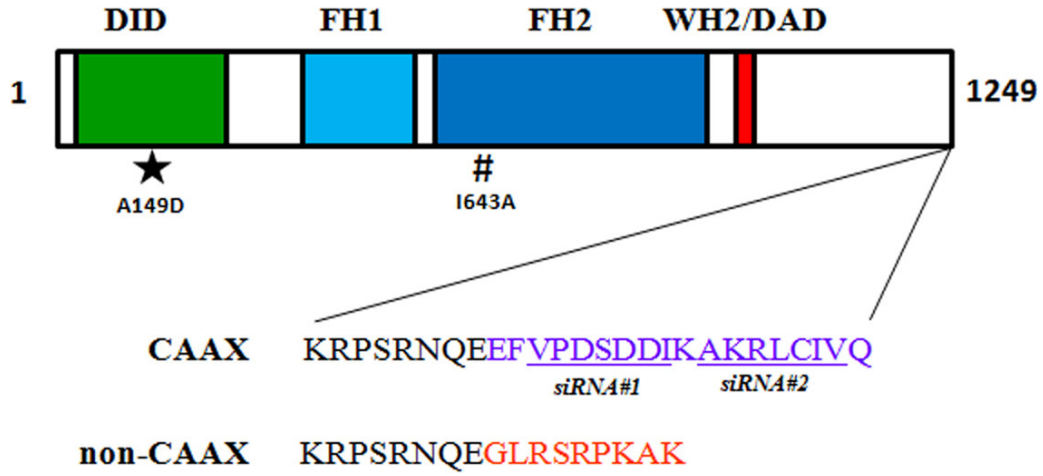

Fig. S1. Domain organization of INF2 and differences between CAAX and nonCAAX splice variants. Bar diagram of INF2 showing relative positions of Diaphanous Inhibitory Domain (DID), Formin Homology 1 domain (FH1), FH2 domain, and Diaphanous Autoregulatory Domain/WASp Homology 2 Domain (DAD/WH2). The positions of the A149 (resulting in constitutive activation when mutated to D) and I643 (compromising actin polymerization and depolymerization when mutated to A) residues are indicated. The sequences of the C-terminal CAAX and nonCAAX variants are also shown. The lines under the CAAX sequence denote the relative positions used for siRNA.

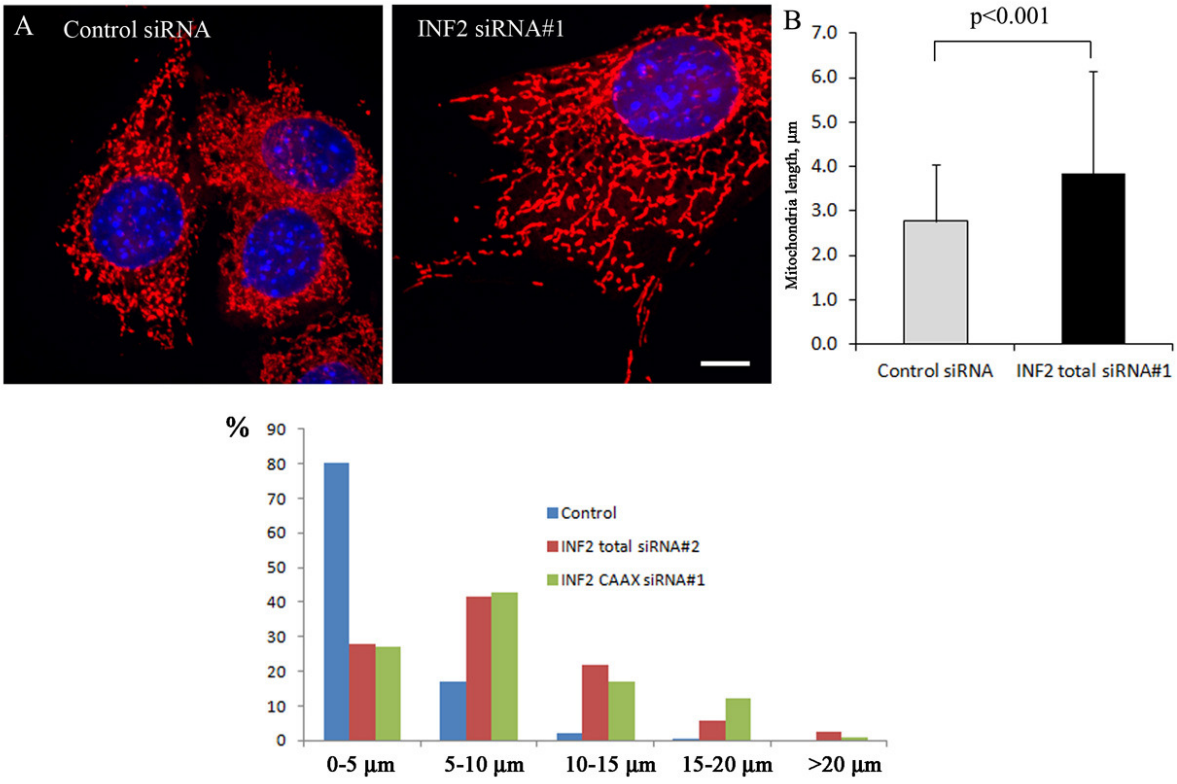

Fig. S2. INF2 suppression in NIH 3T3 cells results in a 1.4-fold increase in mitochondrial size. **(A)** Cells were transfected with control siRNA or siRNA against INF2. After 72 hours, cells were treated with Mitotracker, then fixed and stained with DAPI. Scale bar, 10 µm. **(B)** Mitochondrial length was quantified from maximum intensity projections of confocal images. N = 187-195 mitochondria, error bars, SD. **(C)** Distribution of mitochondrial size in U2OS cells showed significant increase of population of mitochondria greater than 5 µm upon depletion of total or CAAX version of INF2. N = 147-531 mitochondria.

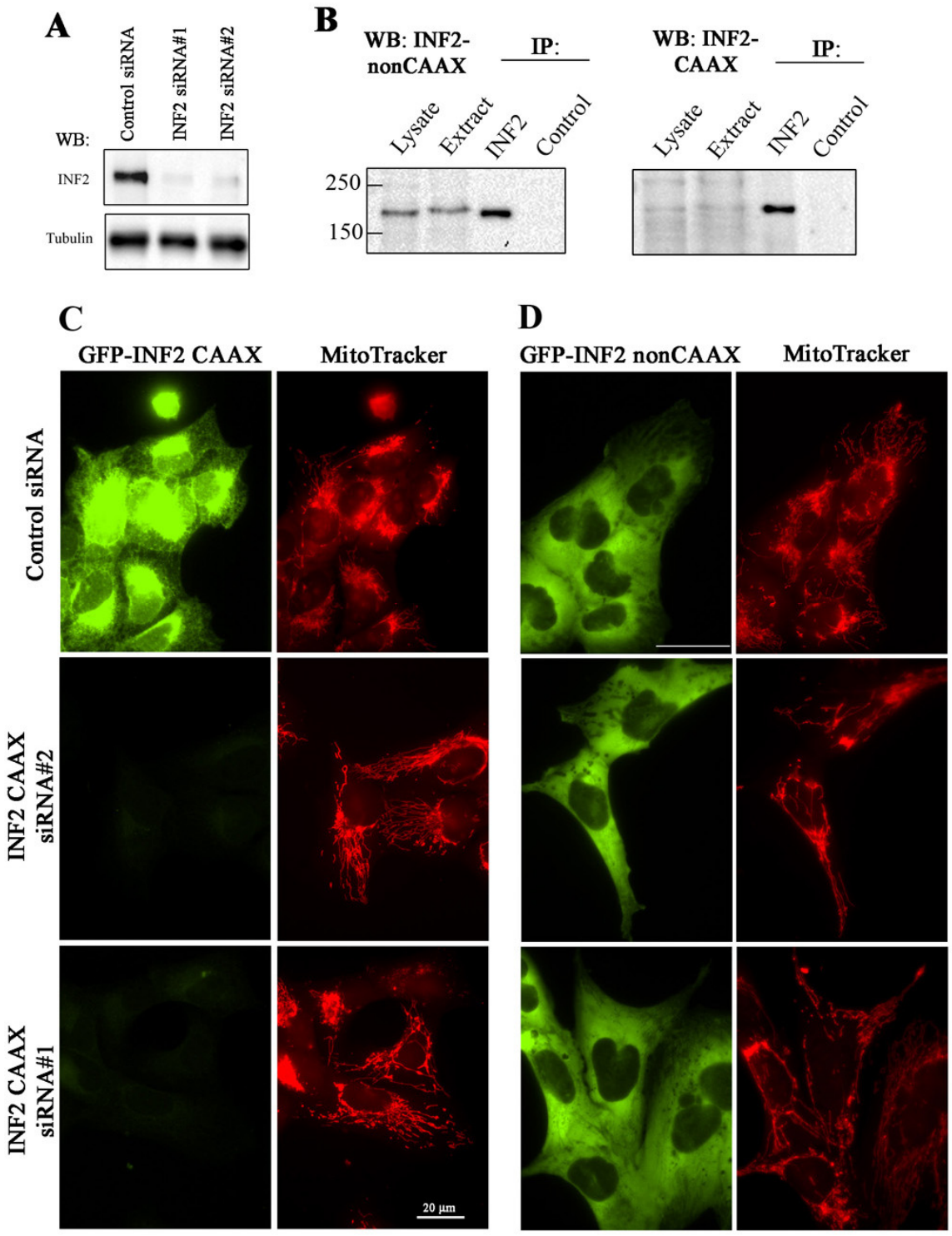

Fig. S3. siRNAs successfully suppress total INF2 or INF2-CAAX expression, respectively. **(A)** Anti-INF2 western blot of U2OS lysates transfected with indicated siRNAs for total INF2 (suppressing both CAAX and nonCAAX) shows 70 and 65 % reduction in INF2 level respectively. **(B)** Western blots of untransfected U2OS lysates and total INF2 immunoprecipitates (anti-INF2 or anti-GFP (negative control)). Blots

probed with anti-INF2-nonCAAX (left) or anti-INF2-CAAX (right). Immunoprecipitations are 40-fold concentrated compared to lysates. **(C-D)** U2OS cell line stably expressing GFP-INF2-CAAX (C) or GFP-INF2-nonCAAX (D) were transfected with two siRNAs directed against the CAAX region. After 72 hours, cells were treated with Mitotracker. Both siRNAs potently reduce the GFP signal in CAAX-, but not nonCAAX-expressing cells. Scale bar, 20 µm. Note that design of siRNAs specific for INF2-nonCAAX is problematic, since the nonCAAX sequence is present in both CAAX and nonCAAX mRNAs.

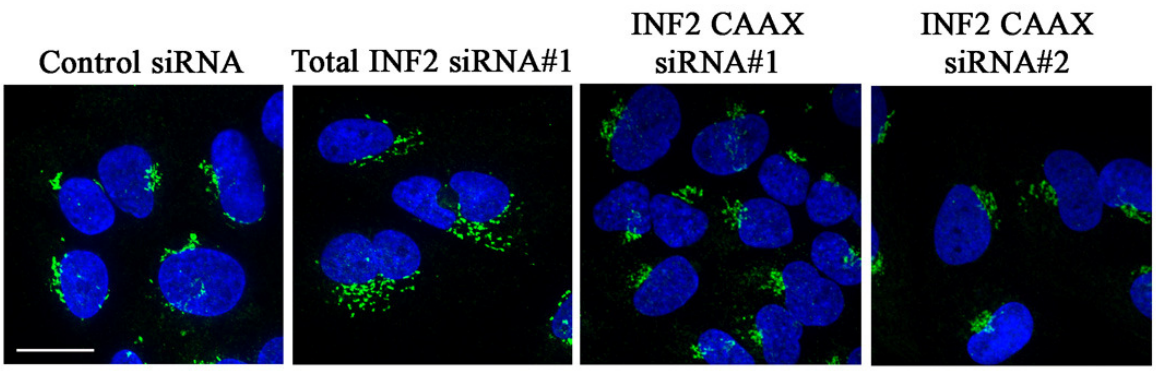

Fig. S4. Suppression of INF2-CAAX does not alter Golgi morphology. U2OS cells were transfected with either control siRNA or siRNAs against total INF2 or INF2-CAAX. 80 hrs post-transfection, cells were fixed and stained with anti-GM130 (green) for Golgi and with DAPI (blue) for nuclei. Maximum intensity projections of confocal z-stacks are shown. Note that suppression of total INF2 causes Golgi dispersion, whereas INF2-CAAX suppression does not. Scale bar, 20 µm.

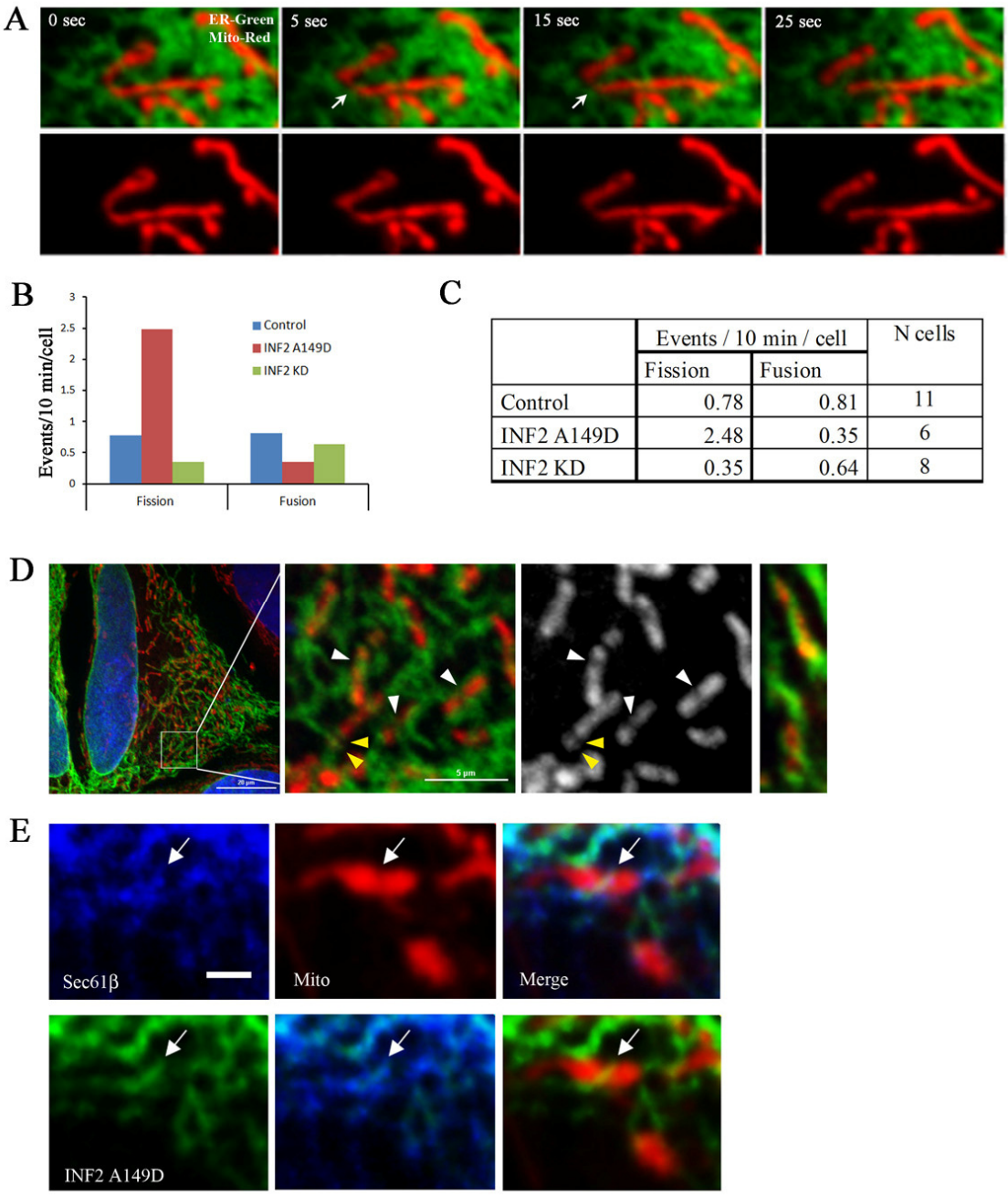

	Events / 10 min / cell		N cells
	Fission	Fusion	
Control	0.78	0.81	11
INF2 A149D	2.48	0.35	6
INF2 KD	0.35	0.64	8

Fig. S5. Effects of INF2-A149D on mitochondrial constriction.
(A) Mitochondrial dynamics (Mito-Red) in U2OS transfected with ER-green. Arrows indicate the fission event. See also Movie S1 Scale bar, 5 µm. **(B, C)** Quantification of mitochondria fission and fusion events from live imaging of cells expressing ER-green (control) or INF2 A149D or total siRNA for INF2. **(D)** Expression of INF2 A149D causes tight association of mitochondria with ER. Zoomed area on the right shows multiple short mitochondria surrounded by INF2-positive ER. Arrowheads indicate constriction (white) or fission sites (yellow) in places where INF2 circumscribes mitochondrion. Quantification of the frequency of constriction events upon

ER/mitochondrial intersection (from movies of mito-dsRed and GFP-ER bound protein) revealed that 68% of A149D cells were constricted versus 35% of ER-green cells (53 events observed). **(E)** INF2 A149D is associated with ER and significantly enriched in places of ER/mito contacts. Arrow point to INF2-enriched part of ER, contacting mitochondrion. Scale bar, 2 μm.

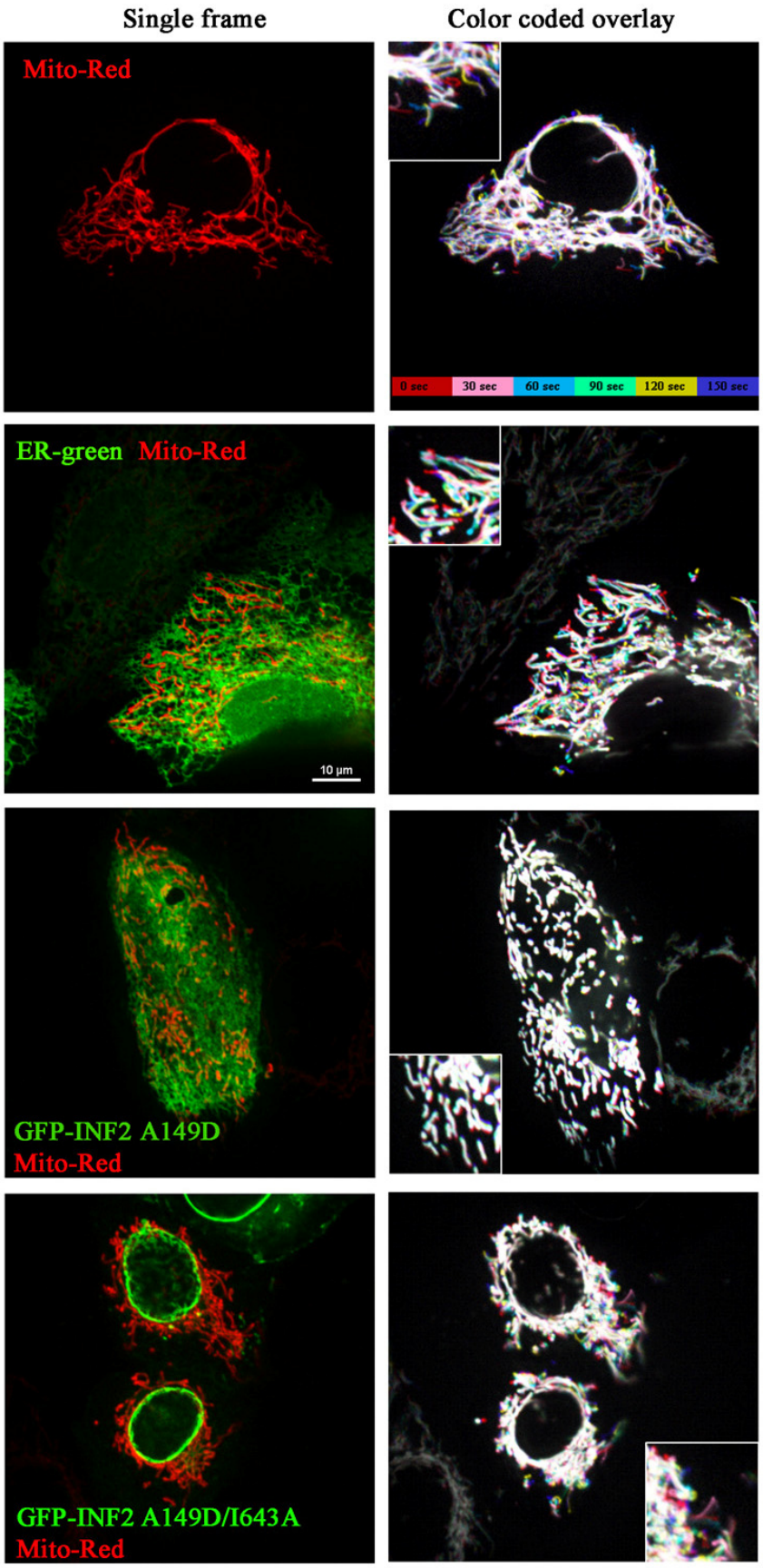
Single frame
Color coded overlay
Mito-Red
0 sec
30 sec
60 sec
90 sec
120 sec
150 sec
ER-green Mito-Red
10 µm
GFP-INF2 A149D
Mito-Red
GFP-INF2 A149D/I643A
Mito-Red

Fig. S6. Expression of INF2-A149D suppress motility of mitochondria.U2OS cells were transfected with Mito-red alone or together with indicated constructs and imaged 24 hrs later. Time sequences with 5 to 11 z-steps (0.2 µm) at each time point for both channels were recorded. Single frames from time lapse sequences of cells are shown in the left panel. The overlays of six color coded frames with 30 sec interval in between from these recorded movies are shown in the right panel. Colors depict various times in the time-lapse, with white indicating that the position was similar in multiple frames. Scale bar, 10 µm. See also movies 3-6.

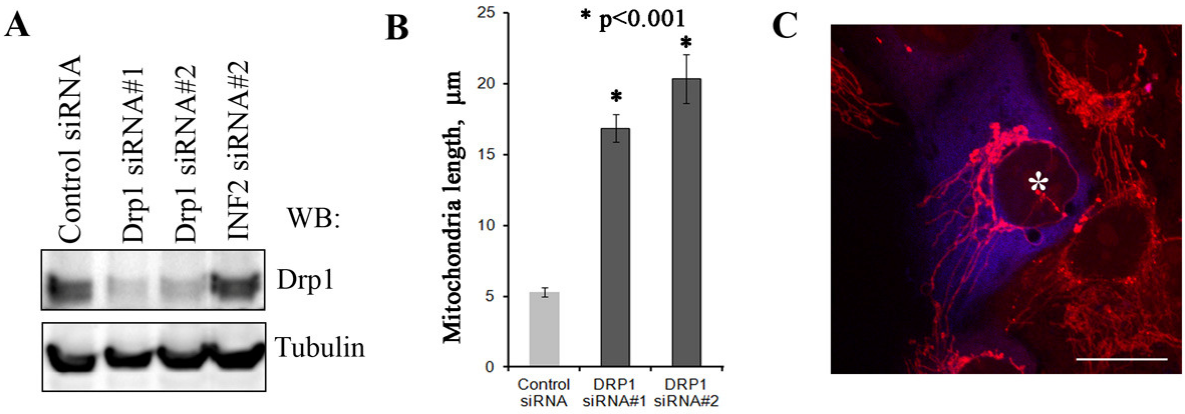

Fig. S7. Suppression of Drp1 or expression of dominant negative Drp1 increases mitochondria size in U2OS cells. **(A)** U2OS were transfected with control siRNA or with siRNAs against INF2. At 80 hrs post-transfection, SDS-PAGE lysates were prepared and examined by western blotting for INF2, Drp1, and tubulin. Quantification of band intensities showed 64 % reduction in Drp1 level for the two siRNAs. Note that Drp1 levels remain relatively constant in the INF2-suppressed conditions. **(B)** Quantification of mitochondrial length in cells expressing two siRNAs for Drp1. Error bars are SEM. **(C)** Drp1 K38E induces elongation of mitochondria. Cells expressing CFP-Drp1 K38E for 18 hrs (blue) were stained with MitoTracker, fixed and analysed on confocal microscope. Note long mitochondria in transfected cell (asterisk). Scale bar, 20 µm.

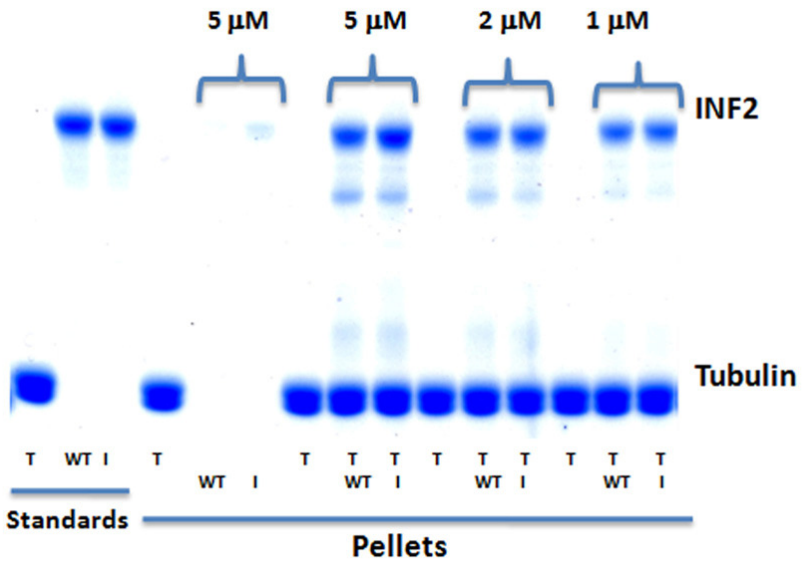

Fig. S8. The I643A mutation does not affect microtubule binding by INF2. Purified bacterially-expressed INF2-FH1FH2C constructs (containing the full C-terminus of the CAAX variant) were examined for co-pelleting with microtubules (0.5 µM tubulin polymerized in the presence of taxol). Standards represent the equivalent of 0.5 µM tubulin or 0.25 µM INF2 in the pelleting assay. Note that the densities of the INF2 bands are very similar for INF2-WT and INF2-I643A at the concentrations tested.

A

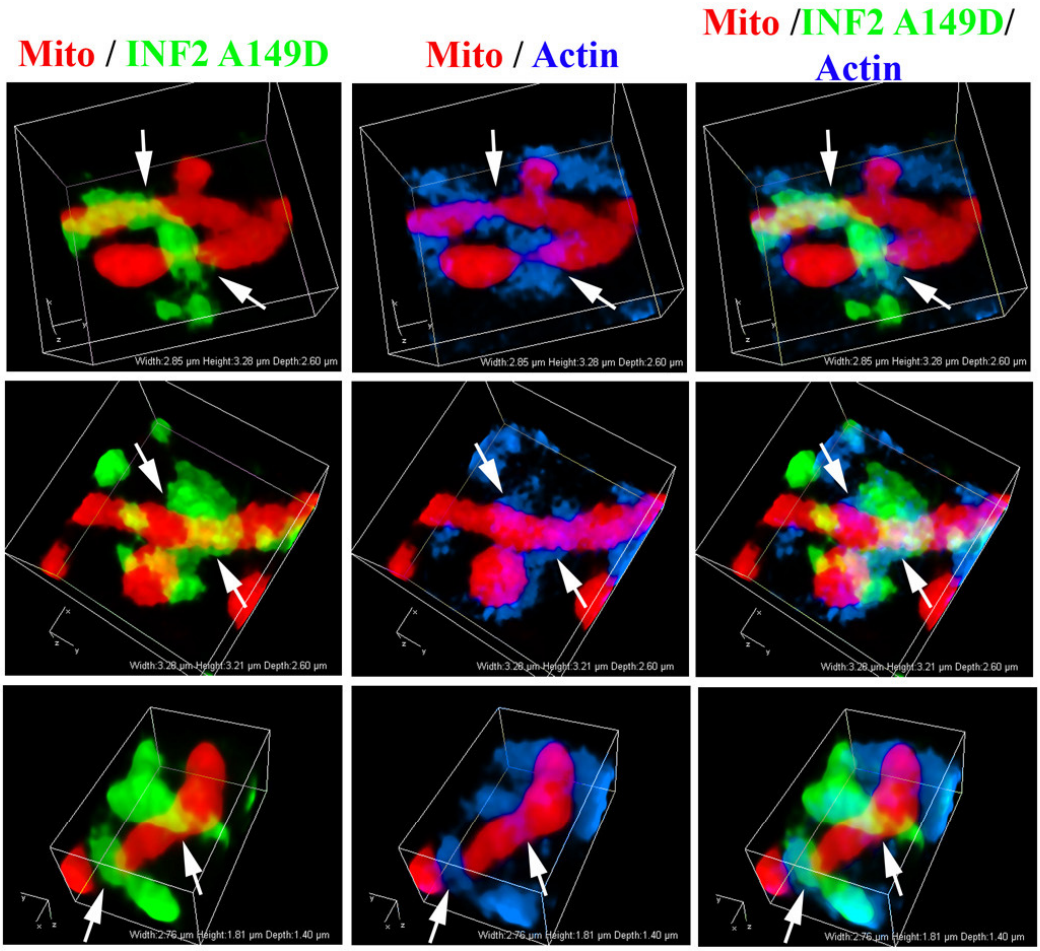

B

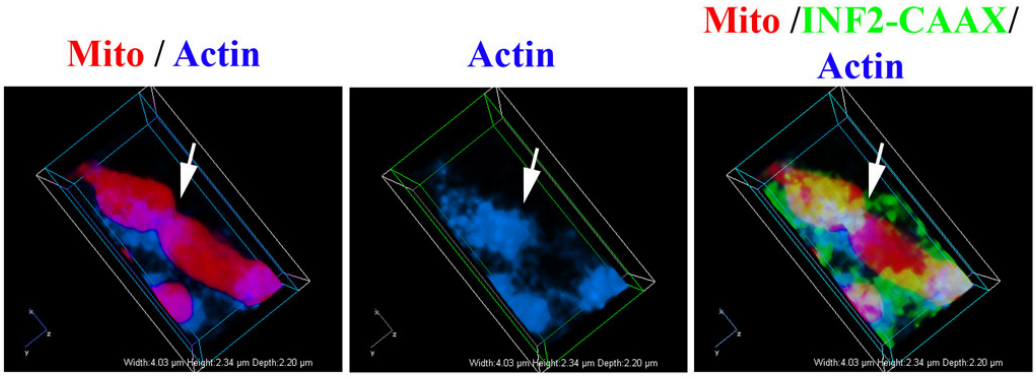

C

	# mitochondria (cells)	# mito/ER contacts	Actin in mito/ER contacts		
			Yes	***No***	***Unclear***
WT	38 (5)	31	5 (16%)	18 (58%)	8 (26%)
A149D	31 (4)	23	15 (65%)	4 (17.5%)	4 (17.5%)

Fig. S9. Examples of ER/mitochondria contact sites enriched in polymerized actin. **(A)** 3D reconstructions of mitochondria from constitutively active A149D-expressing cells. **(B)** 3D reconstruction of a mitochondrion from a WT INF2-expressing cell. Images acquired and processed in the same manner as in Figure 4D of the manuscript. **(C)** Quantification of polymerized actin accumulation at ER/mitochondria contact sites from 3D reconstructions. Mitochondria in cellular regions containing relatively low levels of stress fibers or other actin-based structures were selected. Mito/ER contacts were defined as regions of ER circumscription. Actin presence at these mito/ER contacts was scored positive if actin appeared at this contact in several consecutive Z-frames. "Unclear" indicates that the overall phalloidin staining in the region was too dense to make clear assessment of whether filaments were specifically at the mito/ER contact. See details in Methods.

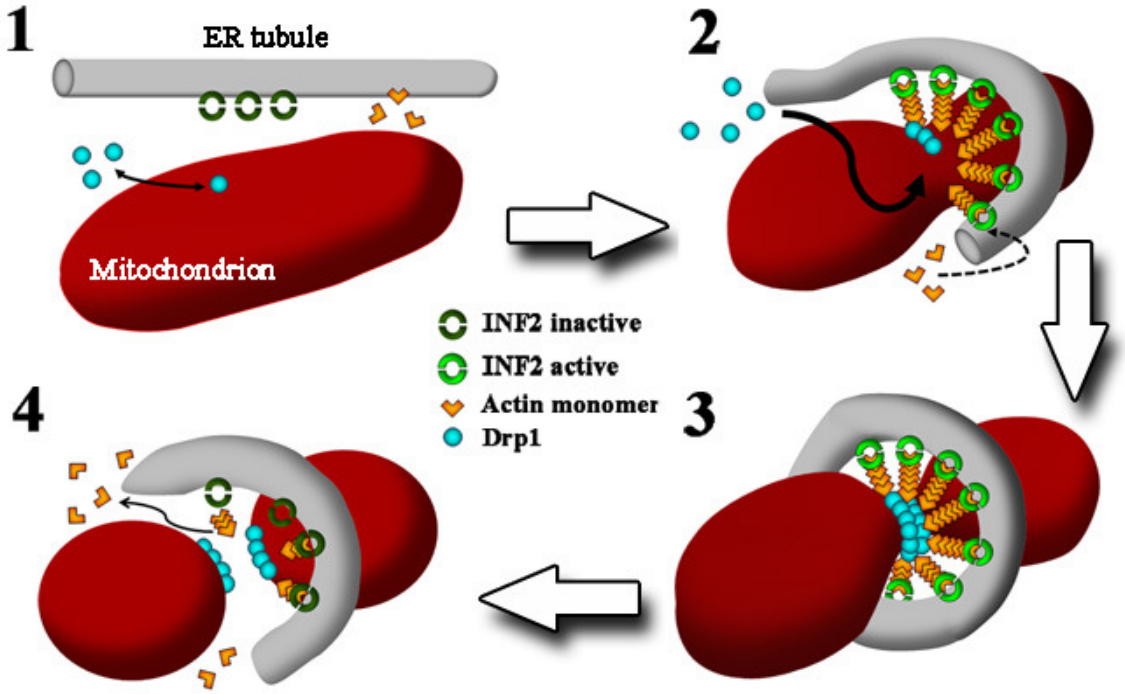

Fig. S10. Model of mitochondrial fission. *Step 1*: Drp1 is in equilibrium on/off mitochondrion. ER-bound INF2 is inactive. *Step 2*: ER-mitochondrion interaction activates INF2 to polymerize actin filaments, which elongate by actin monomer addition to INF2-attached barbed ends. Actin filament pointed ends contact mitochondrion and induce mitochondrial constriction. Mitochondrial constriction shifts Drp1 equilibrium to mitochondrion. *Step 3*: Drp1 assembles helical ring at constriction site. GTP hydrolysis by Drp1 results in further constriction and fission. INF2's severing/depolymerization activity may serve to remove excess filaments during fission. *Step 4*: Post-fission, ER and mitochondrion separate, leading to INF2 inactivation and actin depolymerization. This model is based on three assumptions derived from current knowledge: that INF2 is tightly bound to ER, that INF2 is likely to remain bound to filament barbed ends, and that actin monomer addition takes place at the barbed end. Alternative models involving myosin motor activity are also possible, but this model is the simplest from the available facts. Additional molecules might be required, including: actin bundling molecules, actin filament pointed (minus) end binding molecules, and molecules mediating ER/mitochondria interaction.

Movie S1.
Example of mitochondrial fission in U2OS cell expressing ER-green and mito-dsRed. Time lapse was taken as stack of 6 z-planes every 5 sec, and shown as maximum projections. Time in min.

Movie S2.
Example of mitochondrial fission in U2OS cell expressing GFP-INF2-A149D (green), and mito-dsRed (red). Time lapse was taken as stack of 5 z-planes every 5 sec, and shown as maximum projections. Time in sec.

Movie S3.
Mitochondrial motility in U2OS cell expressing mito-dsRed. Time lapse was taken as stack of 11 z-planes every 5 sec, and shown as maximum projections of best focus planes. Time min:sec.

Movie S4.
Mitochondrial motility in U2OS cell expressing ER-green and mito-dsRed. Time lapse was taken as stack of 9 z-planes every 5 sec, and shown as maximum projections of best focus planes. Time min:sec.

Movie S5.
Mitochondrial motility in U2OS cell expressing GFP-INF2-A149D and mito-dsRed. Time lapse was taken as stack of 7 z-planes every 10 sec, and shown as maximum projections of best focus planes. Time min:sec.

Movie S6.
Mitochondrial motility in U2OS cell expressing GFP-INF2-A149D/I1643A and mito-dsRed. Time lapse was taken as stack of 11 z-planes every 5 sec, and shown as maximum projections of best focus planes. Time min:sec.

References

1. J. Nunnari, A. Suomalainen, Mitochondria: In sickness and in health. *Cell* **148**, 1145 (2012).

2. J. C. Martinou, R. J. Youle, Mitochondria in apoptosis: Bcl-2 family members and mitochondrial dynamics. *Dev. Cell* **21**, 92 (2011).

3. S. Hoppins, J. Nunnari, Mitochondrial dynamics and apoptosis—the ER connection. *Science* **337**, 1052 (2012).

4. R. J. Youle, A. M. van der Bliek, Mitochondrial fission, fusion, and stress. *Science* **337**, 1062 (2012).

5. H. Chen, D. C. Chan, Mitochondrial dynamics—fusion, fission, movement, and mitophagy—in neurodegenerative diseases. *Hum. Mol. Genet.* **18**, (R2), R169 (2009).

6. S. C. Correia *et al*., Mitochondrial importance in Alzheimer's, Huntington's and Parkinson's diseases. *Adv. Exp. Med. Biol.* **724**, 205 (2012).

7. J. A. Mears *et al*., Conformational changes in Dnm1 support a contractile mechanism for mitochondrial fission. *Nat. Struct. Mol. Biol.* **18**, 20 (2011).

8. J. R. Friedman *et al*., ER tubules mark sites of mitochondrial division. *Science* **334**, 358 (2011).

9. A. M. Labrousse, M. D. Zappaterra, D. A. Rube, A. M. van der Bliek, *C. elegans* dynamin-related protein DRP-1 controls severing of the mitochondrial outer membrane. *Mol. Cell* **4**, 815 (1999).

10. A. Legesse-Miller, R. H. Massol, T. Kirchhausen, Constriction and Dnm1p recruitment are distinct processes in mitochondrial fission. *Mol. Biol. Cell* **14**, 1953 (2003).

11. K. J. De Vos, V. J. Allan, A. J. Grierson, M. P. Sheetz, Mitochondrial function and actin regulate dynamin-related protein 1-dependent mitochondrial fission. *Curr. Biol.* **15**, 678 (2005).

12. E. S. Chhabra, H. N. Higgs, INF2 Is a WASP homology 2 motif-containing formin that severs actin filaments and accelerates both polymerization and depolymerization. *J. Biol. Chem.* **281**, 26754 (2006).

13. E. S. Chhabra, V. Ramabhadran, S. A. Gerber, H. N. Higgs, INF2 is an endoplasmic reticulum-associated formin protein. *J. Cell Sci.* **122**, 1430 (2009).

14. V. Ramabhadran, F. Korobova, G. J. Rahme, H. N. Higgs, Splice variant-specific cellular function of the formin INF2 in maintenance of Golgi architecture. *Mol. Biol. Cell* **22**, 4822 (2011).

15. E. J. Brown *et al*., Mutations in the formin gene INF2 cause focal segmental glomerulosclerosis. *Nat. Genet.* **42**, 72 (2010).

16. O. Boyer *et al*., INF2 mutations in Charcot-Marie-Tooth disease with glomerulopathy. *N. Engl. J. Med.* **365**, 2377 (2011).

17. R. Cartoni, J. C. Martinou, Role of mitofusin 2 mutations in the physiopathology of Charcot-Marie-Tooth disease type 2A. *Exp. Neurol.* **218**, 268 (2009).

18. A. Niemann, M. Ruegg, V. La Padula, A. Schenone, U. Suter, Ganglioside-induced differentiation associated protein 1 is a regulator of the mitochondrial network: New implications for Charcot-Marie-Tooth disease. *J. Cell Biol.* **170**, 1067 (2005).

19. A. Vital *et al*., A French family with Charcot-Marie-Tooth disease related to simultaneous heterozygous MFN2 and GDAP1 mutations. *Neuromuscul. Disord.* **22**, 735 (2012).

20. T. Otomo, C. Otomo, D. R. Tomchick, M. Machius, M. K. Rosen, Structural basis of Rho GTPase-mediated activation of the formin mDia1. *Mol. Cell* **18**, 273 (2005).

21. M. J. Woźniak *et al*., Role of kinesin-1 and cytoplasmic dynein in endoplasmic reticulum movement in VERO cells. *J. Cell Sci.* **122**, 1979 (2009).

22. J. Gaillard *et al*., Differential interactions of the formins INF2, mDia1, and mDia2 with microtubules. *Mol. Biol. Cell* **22**, 4575 (2011).

23. V. Ramabhadran, P. S. Gurel, H. N. Higgs, Mutations to the formin homology 2 domain of INF2 protein have unexpected effects on actin polymerization and severing. *J. Biol. Chem.* **287**, 34234 (2012).

24. K. Elgass, J. Pakay, M. T. Ryan, C. S. Palmer, Recent advances into the understanding of mitochondrial fission. *Biochim. Biophys. Acta* **1833**, 150 (2013).

25. B. DuBoff, J. Götz, M. B. Feany, Tau promotes neurodegeneration via DRP1 mislocalization in vivo. *Neuron* **75**, 618 (2012).